Received: 12 April 2019 | Revised: 28 May 2019 | Accepted: 1 June 2019

DOI: 10.1002/jrs.5656

RESEARCH ARTICLE

WILEY Journal of RAMAN SPECTROSCOPY

Surface-enhanced Raman spectroscopy, Raman, and density functional theoretical analyses of fentanyl and six analogs

Ling Wang[1] | Chiara Deriu[1] | Wensong Wu[2] | Alexander M. Mebel[1] | Bruce McCord[1]

[1]Department of Chemistry and Biochemistry, Florida International University, Miami, Florida

[2]Department of Mathematics and Statistics, Florida International University, Miami, Florida

Correspondence
Bruce McCord, Department of Chemistry and Biochemistry, Florida International University, 11200 SW Eighth Street, Miami, FL 33199.
Email: mccordb@fiu.edu

Funding information
NSF IUCRC, Grant/Award Number: 1739805

Abstract

We examined fentanyl and its six analogs using wB97XD/cc-pVTZ density functional theoretical (DFT) calculations as well as Raman and Surface-enhanced Raman spectroscopy (SERS). The *in silico* DFT calculations provided the vibrational frequencies, Raman activities, and normal mode assignment for each analog. Raman spectroscopy can detect crystalline fentanyl analogs but cannot obtain bands for samples in solution. Therefore, we utilized gold/silver nanospheres and gold/silver nanostars to examine them. The gold/silver nanostars provided stronger signals for the fentanyl analogs, and their SERS spectra can easily distinguish these fentanyl analogs from nonfentanyl opioids and other common drugs of abuse using principle component analysis and other statistical tests. Overall, our results demonstrate that SERS shows great potential to distinguish fentanyl analogs and detect trace quantities of these compounds in mixtures of seized drugs.

KEYWORDS

DFT, fentanyl analogs, Raman, SERS

1 | INTRODUCTION

Fentanyl is an opioid that was developed in the 1960s as an alternative to morphine-oxygen anesthesia.[1] It is 80–100 times more potent than morphine, and some of its analogs, such as carfentanil and 3-methylfentanyl, have even higher potency.[2–4] Fentanyl and its analogs have been a continuous threat to public health in the United States since 2005.[5] Over this time, fentanyl abuse has been escalating. In 2016, fentanyl-related opioid abuse resulted in 19,413 overdose deaths, which was 45.9% of all reported drug overdose death.[6,7] Since February 2018, the Drug Enforcement Administration has listed fentanyl as a Schedule II drug and fentanyl-related substances as Schedule I drugs.[8]

Fentanyl and its analogs are rapidly emerging in the drug marketplace. Therefore, there is a need for a quick, sensitive, and highly specific method for the determination of fentanyl and fentanyl analogs in both seized drugs and toxicological samples. Currently, the published screening methods for fentanyls include spot tests,[9] immunoassays,[9–11] ion mobility spectrometry,[12] and GC/MS.[13,14] Other analytical techniques, such as IR, Raman, SERS, and LC/MS have also been studied.[15–20] According to the United National Office on Drugs and Crime report, common immunoassays developed for opioids have high cross-reactivities, making it difficult to detect drug analogs.[10] Surface-enhanced Raman spectroscopy (SERS) is an alternative to current screening methods used for opioids. Unlike normal Raman (NR) spectroscopy, which can only provide information about the molecular structures of analytes at high concentrations, SERS can detect low concentrations, with detection limits (sub ng/ml) that are relevant for toxicological samples.[15]

SERS utilizes metallic nanoparticles creating localized surface plasmon resonance to amplify Raman signals of analytes that are adsorbed or in the vicinity of the nanoparticles. For this reason, SERS is particularly useful as a trace technique for the identification of drugs of abuse.[15] SERS provides molecular recognition based on vibrational spectroscopic identification. Furthermore, Raman spectroscopy can produce complementary data when it is used as a screening procedure for downstream mass spectrometric analysis. Leonard *et al.* described the SERS detection of fentanyl and carfentanil.[16] Haddad and coworkers noted that SERS can detect fentanyl alone as well as in mixtures with heroin.[17] We have analyzed a variety of fentanyl analogs, which were previously reported in drug seizures and verified that SERS can provide a unique and advantageous method to detect these compounds. It is sufficiently flexible to permit quick analysis of newly synthesized compounds with high specificity.

This work focuses on fentanyl, benzylfentanyl (reference standard), and five popular fentanyl analogs reported in forensic casework (shown in Figure 1). We present the results of density functional theory (DFT) calculations for vibrational mode assignments, the Raman (NR) spectra of seven fentanyls in the solid state, and the SERS spectra using two different morphologies of bimetallic (Au/Ag) colloidal nanoparticles—spheroids and stars. In this paper, we also employed principle component analysis (PCA) on the nanostar-based SERS spectra to distinguish fentanyl analogs from other common seized drugs of abuse.

2 | EXPERIMENTAL

2.1 | Chemicals

Tetrachloroauric (III) acid trihydrate ($HAuCl_4 \cdot 3H_2O$) was purchased from Acros Organics (Waltham, MA). Silver nitrate ($AgNO_3$), L-ascorbic acid (L-AA), and magnesium chloride ($MgCl_2$) were purchased from Fisher Chemical (Pittsburgh, PA). Sodium carbonate monohydrate ($Na_2CO_3 \cdot H_2O$) was purchased from Spectrum Chemical (New Brunswick, NJ).

Fentanyl and the analogs acetylfentanyl, acrylfentanyl, benzylfentanyl, butyrylfentanyl, parafluorofentanyl, and furanylfentanyl were purchased from Cayman Chemical (Ann Arbor, MI). Amphetamine, methamphetamine, morphine, hydrocodone, hydromorphone, oxycodone, heroin, codeine, and thebaine were purchased from RBI (Natick, MA).

2.2 | Preparation of bimetallic colloidal nanoparticles

Bimetallic (Au/Ag) colloidal nanoparticles of two different morphologies, nanostars (Au/Ag NS) and nanospheres (Au/Ag NP), were prepared according to a modified version of the method described by He *et al.*[21]; 1 ml of water was mixed with 36 μl of $HAuCl_4$ 10^{-2} M and 2 μl of $AgNO_3$ 10^{-2} M and vortexed for 10 s. Then, the solution was mixed with 6 μl of L-AA 10^{-1} M to prepare the Au/Ag nanostars, or 4 μl of the same solution to prepare

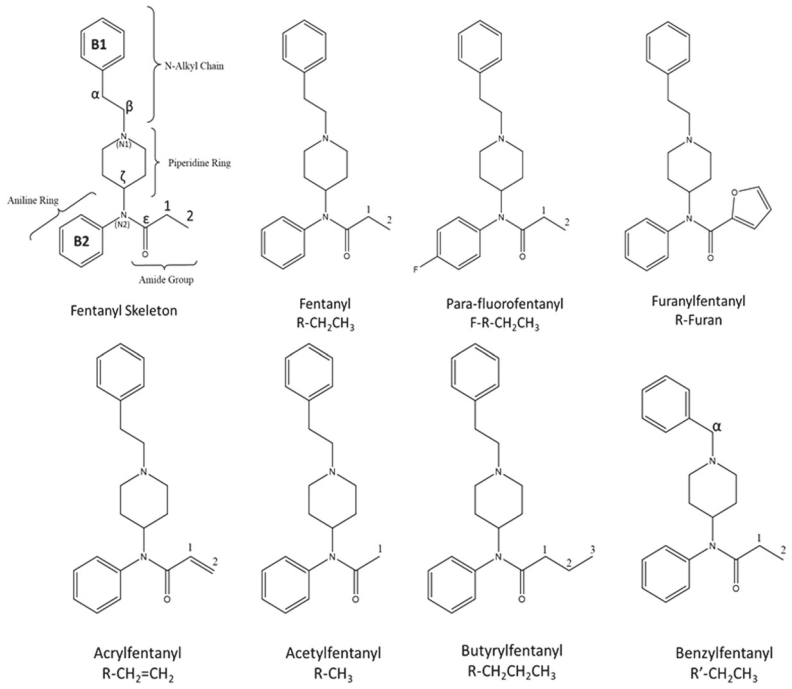

FIGURE 1 Chemical structures of fentanyl skeleton and seven fentanyl analogs

the Au/Ag nanospheres. The mixture was vortexed for another 20 s. Subsequently, 1 μl of Na_2CO_3 1 M was added to stabilize the nanoparticles. The prepared Au/Ag nanostars exhibited a light-blue color with a pH of 6, whereas the Au/Ag nanospheres had a pink color with a pH of 6.5.

2.3 | Preparation of samples for NR and SERS experiments

Fentanyl and its analogs were dissolved in methanol as 1 mg/ml standard solutions. To acquire the NR of drugs in the solid state, a total of 6 μl of standard solutions were deposited onto aluminum foil as three aliquots and allowed to dry. In the solution tests, NR measurements utilized a mixture of 2.5 μl of methanolic standard solutions and 247.5 μl of water. For the SERS measurements, 2.5 μl of 1.67 M magnesium chloride were added to 245 μl of colloidal nanoparticles, which were allowed to aggregate for 5 min. Then, a 2.5 μl aliquot of each drug sample was added to the aggregated colloidal sol. This mixture was incubated for another 5 min and then transferred to a 96-wells quartz microtiter plate. SERS measurements were performed at the 15th, 20th, 25th, and 30th minute time points. Unless specified otherwise, the final concentration of drug used in this study was 10 μg/ml.

2.4 | Instrumentation

NR and SERS spectra were collected using a Perkin Elmer 400F benchtop Raman spectrometer fitted with an excitation laser at 785 nm (350 mW power at the source, 100 mW power at the sample, 0.05 nm FWHM) and an air-cooled (−50°C) CCD detector. Both NR and SERS spectra were recorded by averaging four accumulations, each of 10-s exposure time. All spectra displayed in this paper were baseline corrected and normalized by the intensity of the band at 3,200 cm^{-1}, which was assigned to ν (OH) of water.

2.5 | DFT calculations

The Gaussian 09 package was used for all DFT calculations.[22] The Raman frequency calculations were performed after prior optimization of molecular geometries. This was done by utilizing the hybrid exchange correlation functionals of B3LYP[23,24] and wB97XD[25] coupled with the basis sets of 6-311G** and cc-pVTZ,[26] respectively. The obtained Raman frequencies and activities were converted to simulated spectra by utilizing MultiWFN[27] (ν_{exc} 12738.85 cm^{-1}, T 294.15 K, standard broadening Lorentzian function), whereas the optimized geometry was visualized by Molden 5.0.[28]

3 | RESULTS AND DISCUSSIONS

3.1 | DFT calculations

The fentanyl analogs shown in Figure 1 illustrate the characteristic structures and the labeling of the fentanyl skeleton. For simplicity, we have designated the phenyl ring as *B1*, the aniline ring as *B2*, and the piperdine ring as *pip*. The optimal geometry and vibrational frequencies of benzylfentanyl were computed using B3LYP/6-311G**, which provided a set of Raman frequencies with the simulated spectrum closely resembling the experimental one. When the vibrational frequencies for fentanyl were calculated using the B3LYP/6-311G** and B3LYP/cc-pVTZ methods, the simulated spectrum appeared to be shifted relative to the experimental one in multiple regions, and exhibited a quadruple peak in the 1,100–900-cm^{-1} range (Figure S1). In contrast, the experimental spectrum featured a double band in this range, and the intensities of the corresponding constituent bands at 1,066 cm^{-1} and 1,031 cm^{-1} were reversed. Furthermore, we examined wB97XD/cc-pVTZ as an alternative method for the geometry optimization and the calculation of frequencies. Using this approach, the simulated spectrum of fentanyl with a scaling factor of 0.9660[29] provided good agreement with experimental data. Therefore, we used this same wB97XD/cc-pVTZ computational method to calculate the remaining fentanyl analogs.

3.2 | Evaluation of scaling factors

Table 1 presents the selected bands that were used to calculate the scaling factors between the calculated DFT spectra and the NR spectra. In this study, we did not split the scaling factors to the high/low frequency region because we only have seven analogs, and the errors in the calculated frequencies were lower than 7.6%.

It is interesting to compare the scaling factors derived from fentanyl analogs to predict or assign an unknown spectrum of a new analog. Here, we selected five fentanyl analogs (fentanyl, benzylfentanyl, parafluorofentanyl, acrylfentanyl, and butyrylfentanyl) to compare with acetylfentanyl (an analog without special functional groups) and furanylfentanyl (an analog with a special functional group). The specific scaling factor was calculated as the average of the ratios between the experimental and computed frequencies, $\lambda = \nu^{exp}/\omega^{cal}$.[30] With the selected five analogs, the average scaling factor was 0.9606, and the tested acetylfentanyl and furanylfentanyl

TABLE 1 Calculated DFT, experimental normal Raman, and SERS vibrational frequencies of fentanyl analogs and assignments of vibrational normal modes

Butyrylfentanyl	**Calculated**		**Experimental**	
Description	**Mode**	**DFT × 0.9536**	**Raman/cm^{-1}**	**SERS/cm^{-1}**
ν (C═C)$_{B1}$	131	1,610 s	1,596 m	1,600 w
τ (CH$_2$)$_\alpha$, ν (C–C)$_{B1}$	129	1,587 w	1,584 w	1,582 vw
σ (CH$_2$)$_{pip}$, σ (CH$_2$)$_\beta$	117	1,432 s	1,442 w	1,444 w
τ (CH$_2$)$_{pip}$, τ (CH$_2$)$_{\alpha,\beta}$	93	1,223 w	1,206 w	1,202 w
ν (B1-C-C), σ (CH)$_{B1}$, τ (CH$_2$)$_{pip}$, τ (CH$_2$)$_{\alpha,\beta}$	90	1,190 m	1,172 vw	1,174 w
τ (CH$_2$)$_{pip}$, τ (CH$_2$)$_{\alpha,\beta}$	87	1,164 m	1,158 w	1,158 vw
ν (CCC)$_{alkyl}$	72	1,017 s	1,028 m	1,028 m
δ (C═C)$_{B1}$	65	984 s	1,004 s	1,004 s
τ (CH$_2$)$_{pip}$, ρ (CH$_2$)$_{pip}$, ν (C$_1$-C$_\varepsilon$-N2),	61	958 w	978 vw	980 vw
ν (C$_{B1}$-C$_\alpha$-C$_\beta$), ρ (CH$_2$)$_{pip}$	51	826 m	832 m	832 w
δ (C$_{B2}$-N1-C), δ (ring)$_{pip}$, β (ring)$_{B2}$, δ (CCC)$_{alkyl}$	40	647 w	654 vw	656 vw
δ (ring)$_{B2}$	38	614 m	622 m	622 vw
Acrylfentanyl	**Calculated**		**Experimental**	
Description	**Mode**	**DFT × 0.9573**	**Raman/cm^{-1}**	**SERS/cm^{-1}**
ν (C═C)$_{B2}$	118	1,610 s	1,618 m	1,602 w
σ (CH$_2$)$_{pip}$, δ (CH)$_{B1}$	110	1,445 m	1,462vw	—
ν (HC═CH$_2$), τ (CH$_2$)$_{pip}$, τ (CH$_2$)$_\beta$, τ (CH$_2$)$_{acryl}$, τ (CH)$_{acryl}$	94, 95	1,297 m	1,276 s	1,278 vw
τ (CH$_2$)$_{pip}$, τ (CH$_2$)$_\alpha$, ν (C-N2-C-C), τ (CH$_2$)$_\beta$, δ (CH)$_{B2}$	88	1,232 m	1,208 w	1,202 w
τ (CH$_2$)$_{pip}$, τ (CH$_2$)$_{\alpha,\beta}$, ν (N1-C-C-C)	85	1,194 m	1,164 w	1,158 vw
ν (C═C)$_{B1}$, δ (C-H)$_{B1}$	69	1,020 s	1,038 w	1,030 m
δ (C═C)$_{B1}$, γ (CH)$_{B2}$	61, 62	987 s	1,008 s	1,004 s
δ (C–C–C)$_{pip}$, ρ (CH$_2$)$_{pip}$	47	814 m	834 m	830 w
ρ (CH$_2$)$_{pip}$, ρ (CH$_2$)$_{acryl}$	41	742 w	748 m	748 w
δ (C═C)$_{B2}$, ρ (CH$_2$)$_{acryl}$, ρ (CH$_2$)$_{pip}$	38	664 w	646 vw	646 vw
δ (ring)$_{B1,B2}$	35	614 s	626 m	620 w
Benzylfentanyl	**Calculated**		**Experimental**	
Description	**Mode**	**DFT × 0.9592**	**Raman/cm^{-1}**	**SERS/cm^{-1}**
ν (C═C)$_{B2}$	116	1,610 m	1,598 m	1,602 w
ν (C═C)$_{B1}$	115	1,597 w	1,586 m	1,586 m
τ (CH$_2$)$_{pip}$, τ (CH$_2$)$_\alpha$	76	1,144 w	1,160 m	1,158 w
δ (CH)$_{B2}$, ν (C═C)$_{B2}$	65	1,017 m	1,030 s	1,028 s
δ (C═C)$_{B2,B1}$, ρ (CH$_2$)$_\alpha$	58, 59	990 s	1,004 s	1,004 s
ρ (CH$_2$)$_{pip}$	49	860 m	834 w	832 w
ω (CH$_3$), ρ (CH$_2$)$_{pip}$, ν (C-N2-C), δ (C-C$_1$-C$_2$)	40	731 s	746 s	746 m
δ (ring)$_{B1}$	35	619 m	622 m	620 w

Acetylfentanyl	Calculated		Experimental	
Description	Mode	DFT × 0.9696	Raman/cm^{-1}	SERS/cm^{-1}
ν (C=C)$_{B1}$	117	1,636 m	1,598 w	1,600 w
ν (C=C)$_{B2}$	115	1,611 w	1,584 w	1,582 w
δ (CH$_2$)$_\beta$, σ (CH$_3$), σ (CH$_2$)$_{pip}$	106	1,460 m	1,460 w	1,442 vw
τ (CH$_2$)$_{pip}$, ν (C-N2-C), δ (CH)$_{B2}$	85	1,259 m	1,284 w	1,282 vw
τ (CH$_2$)$_{pip}$, ω (CH$_2$)$_\beta$	83	1,235 w	1,248 w	1,248 vw
ν (B1-C), δ (C-H)$_{B1}$, ω (CH$_2$)$_\alpha$	81	1,195 m	1,206 m	1,204 w
ν (C-N1-C), τ (CH$_2$)$_{pip}$, δ (C-H)$_{B1,B2}$	77	1,169 w	1,176 vw	1,174 vw
δ (C–H)$_{B2}$	74	1,153 w	1,160 vw	1,158 vw
ν (C–C)$_{pip}$	63	1,024 m	1,034 s	1,030 m
δ (C=C)$_{B2}$	59	1,000 s	1,002 s	1,004 s
ν (B1-C-C), ρ (CH$_2$)$_{pip}$, β (ring)$_{B1}$	45	818 s	832 m	832 m
γ (C–H)$_{B1}$, γ (C-H)$_{B2}$, ρ (CH$_2$)$_{pip}$, ν (C-C-N2), ρ (CH$_3$)	40	726 m	742 m	744 m
ν (C-N2-C), ν (C=C-N2), δ (ring)$_{B2}$	37	666 m	652 w	660 vw
δ (ring)$_{B1}$	35	624 m	628 w	622 vw

Parafluorofentanyl	Calculated		Experimental	
Description	Mode	DFT × 0.9593	Raman/cm^{-1}	SERS/cm^{-1}
ν (C=C)$_{B1}$	124	1,616 s	1,602 m	1,600 m
ν (C=C)$_{B2}$	123	1,598 m	1,586 w	1,582 vw
σ (CH$_2$)$_\beta$, σ (CH$_2$)$_{pip}$, δ (CH)$_{B1}$	114	1,443 s	1,466 m	1,470 w
ν (C$_\alpha$-B1), ω (CH$_2$)$_\alpha$, ρ (CH)$_{B1}$	85	1,192 m	1,204 m	1,204 m
τ (CH$_2$)$_{pip}$, τ (CH$_2$)$_{\alpha,\beta}$	84	1,172 m	1,158 m	1,158 m
σ (CH)$_{B2}$, τ (CH$_2$)$_{pip}$, τ (CH$_2$)$_{\alpha,\beta}$	81	1,143 m	1,152 w	—
ν (C=C)$_{B1}$	70	1,023 m	1,034 m	1,030 m
δ (C=C)$_{B1}$	65	990 s	1,002 s	1,002 s
ν (N1-C$_\alpha$-C$_\beta$), ρ (CH$_2$)$_{pip}$, γ (C-H)$_{B2}$, δ (C-C$_1$-C$_2$)	52	828 s	824 s	824 s
ρ (CH$_2$)$_{pip}$, ν (C-N2-C), ν (C$_\varepsilon$-C$_1$-C$_2$), ρ (CH$_3$)	41	655 w	642 m	622 w
δ (ring)$_{B2}$	40	637 w	622 m	621 m

Fentanyl	Calculated		Experimental	
Description	Mode	DFT × 0.9573	Raman/cm^{-1}	SERS/cm^{-1}
ν (C=C)$_{B1}$	124	1,629 s	1,606 w	1,600 w
ν (C=C)$_{B1}$	122	1,605 w	1,586 w	1,588 w
δ (H-C-N2)	108	1,425 m	1,456 w	1,442 w
ν (N1-C-C-C$_{B1}$); τ (CH$_2$)$_\alpha$	85	1,206 m	1,206 w	1,202 w
δ (CH)$_{B1,B2}$	80	1,154 w	1,160 m	1,158 vw
ν (C=C)$_{B1,B2}$, δ (CH)$_{B1,B2}$	70	1,034 m	1,034 m	1,030 m
δ (C=C)$_{B2}$, ν (C$_\varepsilon$-C$_1$-C$_2$)	62	996 s	1,002 s	1,004 s
ρ (CH$_2$)$_{pip}$, ν (C$_\varepsilon$-C$_1$-C$_2$)	57	961 w	964 vw	970 w
ν (C$_{B1}$-C$_\alpha$-C$_\beta$-N1), β (ring)$_{B1}$	49	830 m	830 m	832 w
τ (CH$_3$), ρ (CH$_2$)$_{pip}$, δ (C$_\varepsilon$-C$_1$-C$_2$)	42	732 m	742 m	746 w
δ (ring)$_{B1,B2}$, ρ (CH$_2$)$_{alkyl}$, ρ (CH$_3$)	37	622 m	622 m	620 w

Furanylfentanyl Description	Calculated Mode	Calculated DFT × 0.9536	Experimental Raman/cm^{-1}	Experimental SERS/cm^{-1}
ν (C═C)$_{furane}$	125	1,596 s	1,602 m	1,599 w
ν (C═C)$_{furane}$	122	1,496 s	1,472 s	1,468 s
ω (CH$_2$)$_{pip}$, ω (CH$_2$)$_{\beta}$	112	1,393 m	1,388 m	1,390 w
τ (CH$_2$)$_{pip}$, δ (CH)$_{furane}$, δ (C$_{furane}$-C$_{\varepsilon}$-N2-C$_{pip}$)	92	1,205 w	1,208 w	1,204 w
δ (CH)$_{B2}$	74	1,025 m	1,034 w	1,030 m
δ (C═C)$_{B1}$	67	996 s	1,004 s	1,004 s
δ (ring)$_{furane}$, δ (ring)$_{pip}$	56	877 w	886 w	886 w
δ (C$_{B2}$-N2-C$_{\varepsilon}$-C$_{furane}$), δ (C$_{B2}$-N2-C$_{pip}$), γ (CH)$_{B2}$	51	826 m	826 w	828 w
ρ (CH$_2$)$_{\alpha,\beta}$, ρ (CH$_2$)$_{pip}$	49	788 w	794 w	790 vw
δ (ring)$_{B1}$	39	622 vw	622 w	620 w

Def: ν: stretching; δ: in-plane bending; σ: scissoring; ρ: rocking. γ: out-of-plane bending; τ: twisting; ω: wagging. β: ring breathing.

Abbreviations: DFT, density functional theoretical; SERS, surface-enhanced Raman spectroscopy.

had errors lower than 3%. Therefore, the wB97XD/cc-pVTZ method can be used to predict unknown spectra if the required accuracy is not high. The errors in the predicted frequencies should be less than 4%.[30]

3.3 | Effects of nanomaterial morphology on SERS detection

It is known that the morphology of nanoparticles and their aggregation state affects the SERS response.[31] This was verified by studying the SERS spectra of acrylfentanyl and benzylfentanyl at a concentration of 10 ng/ml utilizing both Au/Ag nanospheres and Au/Ag nanostars. The spectra presented in Figure S2 demonstrates the superiority of the spiked morphology in producing a SERS enhancement with λ_{exc} 785 nm. For both analogs, this is reflected in an improved spectral quality and a higher signal-to-noise ratio. Moreover, the intensity of the characteristic band at 1,004 cm^{-1} was 4.36 times (benzylfentanyl) and 1.73 times (acrylfentanyl) higher when using the Au/Ag nanostars than that obtained with the Au/Ag nanospheres. In the case of benzylfentanyl, the use of nanostars facilitated the observation of bands at 1,158 and 832 cm^{-1}, which were otherwise undetectable. Hence, the Au/Ag nanostars were used exclusively to detect the rest of fentanyl analogs in this study.

3.4 | Raman and SERS spectra of fentanyl analogs

Figures 2, 3a–f, and 4, as well as Table 1 show the characteristic bands in Raman, SERS, and DFT-simulated spectra. These figures and this table illustrate the differences

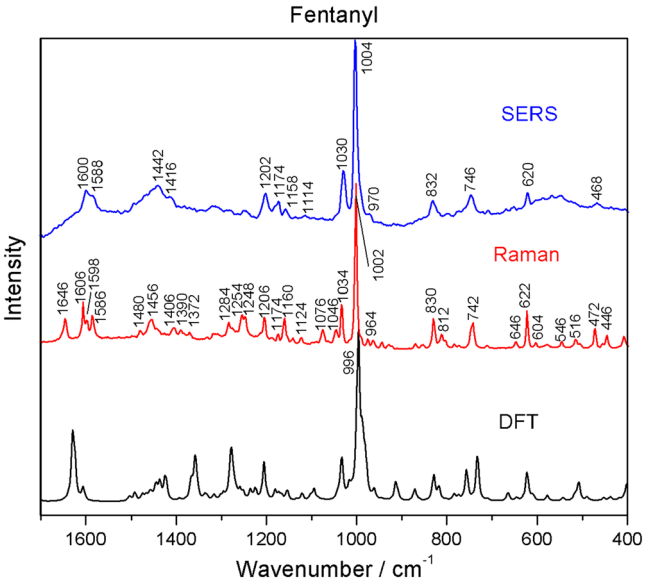

FIGURE 2 Calculated and experimental spectra of fentanyl [Colour figure can be viewed at wileyonlinelibrary.com]

between the simulated spectra and the NR spectra for each fentanyl analog in terms of wavenumber shifts and relative intensities. The main differences between the NR and the SERS spectra consisted of changes in intensities rather than in shifts in wavenumbers. We tried solution tests with NR; however, the highest concentrations we could prepare were 500 μg/ml of morphine and 50 μg/ml of fentanyl. Even these concentrations did not provide spectra.

The seven fentanyl analogs were characterized by an ensemble of bands at 1,620–1,580 cm^{-1}. In the Raman spectra, butyrylfentanyl, parafluorofentanyl, and furanylfentanyl produced two bands, whereas fentanyl, benzylfentanyl, acetylfentanyl, and acrylfentanyl

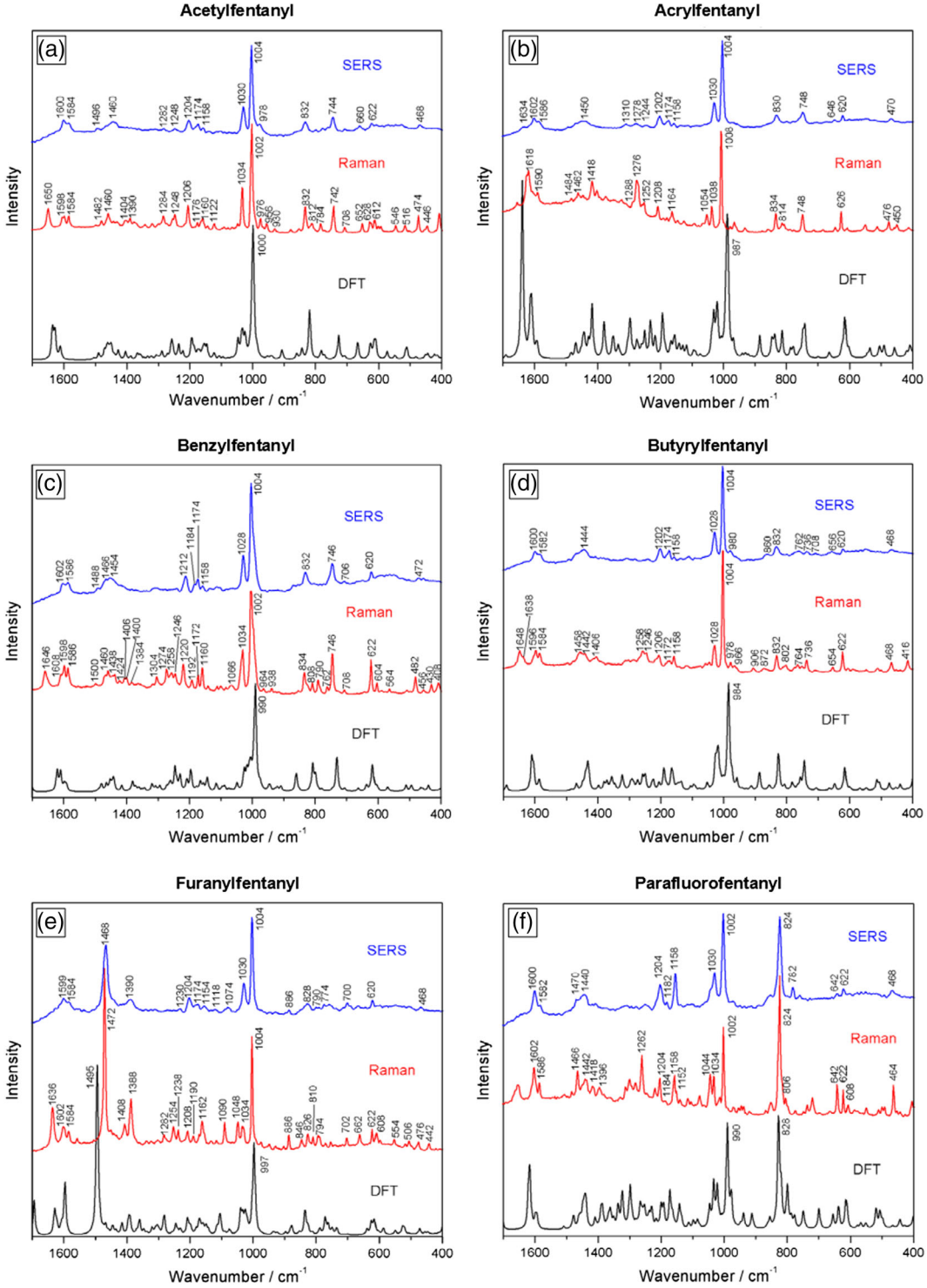

FIGURE 3 Calculated and experimental spectra of six fentanyl analogs [Colour figure can be viewed at wileyonlinelibrary.com]

produced three bands. However, in the SERS spectra for these compounds, the band at the highest frequency (~1,650 cm^{-1}) was absent, and the two remaining bands appeared at ~1,600 and 1,580 cm^{-1}. This spectral pattern was shown by all analogs, except for acrylfentanyl, which retained a higher frequency shoulder at 1,634 cm^{-1}.

In the region from 1,550 to 1,350 cm^{-1}, all tested compounds except furanylfentanyl showed multiple weak bands in their NR spectra. Furanylfentanyl instead had its most intense band in this region (1,472 cm^{-1}), along with a weak band at 1,388 cm^{-1}. This was also observed in the SERS spectrum of furanylfentanyl. However, the remaining analogs exhibited an SERS profile in this region that was not characterized by resolved bands. Instead, a broad and weak band centered at ~1,444 cm^{-1} was observed. This broad band showed a

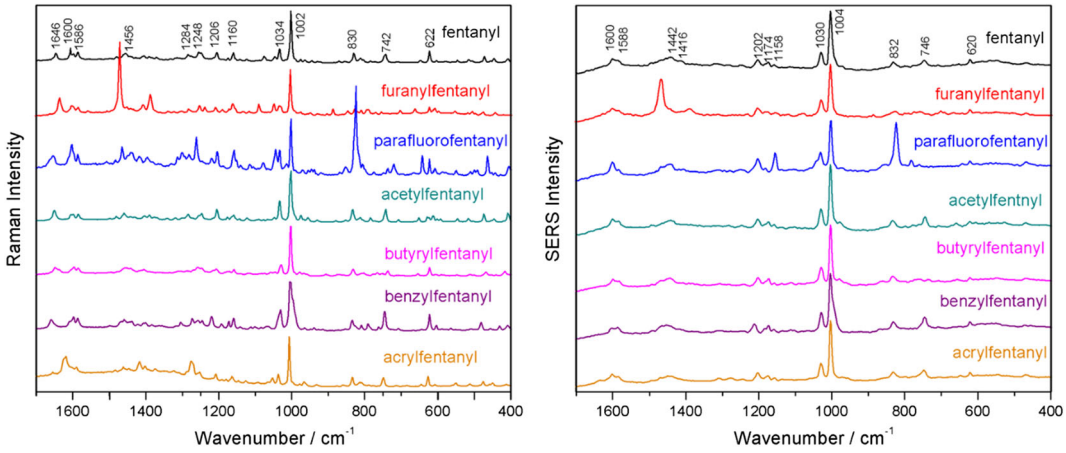

FIGURE 4 Comparison of Raman and surface-enhanced Raman spectroscopy spectra of seven fentanyl analogs [Colour figure can be viewed at wileyonlinelibrary.com]

shoulder at 1,470 cm^{-1} in the parafluorofentanyl SERS spectrum, whereas two overlapping bands at 1,454 and 1,466 cm^{-1} appeared in the benzylfentanyl SERS spectrum.

In the range from 1,350 to 1,050 cm^{-1}, medium and weak Raman bands were observed, the intensities of which was much weaker in the respective SERS profiles. All fentanyl analogs displayed bands at 1,184 and 1,158 cm^{-1} whereas benzylfentanyl had an additional weak band at 1,212 cm^{-1}. The other six fentanyl analogs were characterized by an additional band at 1,204 cm^{-1}. Acrylfentanyl had a triple band at 1,310, 1,278, and 1,244 cm^{-1}.

Two characteristic bands of fentanyl-related compounds were observed at ~1,004 and 1,030 cm^{-1} in both Raman and SERS spectra. Moreover, the first characteristic band exhibited a shoulder at 970 cm^{-1} in fentanyl, at 978 cm^{-1} in acrylfentanyl and at 980 cm^{-1} in butyrylfentanyl.

From 950 to 400 cm^{-1}, the fentanyl analogs had many weak and very weak bands in both SERS and Raman spectra. Weak bands appeared at ~832 and ~620 cm^{-1}. Only para-fluorofentanyl had a very strong band at 824 cm^{-1}. Furanylfentanyl had weak bands at 866 and 700 cm^{-1}; acrylfentanyl, acetylfentanyl, fentanyl, and benzylfentanyl had a band at 746 cm^{-1}. Acetylfentanyl had a very weak band at 660 cm^{-1}, and acrylfentanyl had one at 646 cm^{-1}. A table summarizing the characteristic bands for all fentanyl analogs is given in the supplementary information (Table S1).

3.5 | Vibrational characterization

Fentanyl analogs have two monosubstituted benzene rings, *B1* and *B2*. These are located at the two ends of the molecules and therefore do not interact with each other.[16] The aromatic ring *B1* connects to C_{α}, acting as a benzyl group. The *N2* atom is connected to a *pip* ring, another benzyl ring *B2,* forming an aniline group, and to a carbonyl functional group, forming an amide. The selected fentanyl analogs had similar chemical structures, so their Raman and SERS spectra exhibited many similarities. We compared the NR with the DFT-simulated and with the SERS spectra, in particular, the bands at ~622, ~832, ~1,004, ~1,034, ~1,160, ~1,174, ~1,206, ~1,440–1,460, ~1,582–1602 cm^{-1}, and assigned vibrational frequencies.

First, we compared the results of the NR spectra of solid samples with the simulated spectra (Table 1). The ring C═C stretches from two monosubstituted aromatic rings, *B1* and *B2*, contributed to the strongest band at ~1,004 cm^{-1} in both NR and SERS spectra for all seven fentanyl analogs. This band can be used to distinguish the fentanyl analogs from common opiates, for example, morphine, hydrocodone, hydromorphone, oxycodone, heroin, codeine, and thebaine. The other characteristic band, ~1,034 cm^{-1} in NR spectra and ~1,030 cm^{-1} in SERS spectra, was also observed in all seven fentanyl analogs. This band was the result of different vibration modes for each fentanyl analog (Table 1). For fentanyl, benzylfentanyl, acrylfentanyl, parafluorofentanyl, and furanylfentanyl, this band was the result of C═C stretches and C–H bends in the aromatic rings. As for butyrylfentanyl, the band was assigned to the C–C–C stretch of the side chain in the amide group. In the NR spectrum, this band was shifted to a slightly lower wavenumber and had medium intensity. Acetylfentanyl has only one carbon in the side chain of the amide group, and the strong band at ~1,030 cm^{-1} is the result of a C–C stretch in the *pip* ring.

At high wavenumbers, all seven fentanyl analogs had a double band at ~1,586 and 1,602 cm^{-1} due to a C═C

stretch of the aromatic rings. In addition to this double band, butyrylfentanyl had a CH_2 twist at the C_α and C_β atoms, and furanylfentanyl had extra in-plane bending of C–H groups for both the *furane* and *pip* rings. Theoretically, the C═C stretch of the aromatic rings can also produce a moderate band at ~1,450 cm^{-1}. Fentanyl analogs had other bands in this region, which were found to be related to the C–H in-plane bend in *B1* (parafluorofentanyl), the CH_2 scissoring in *pip* (fentanyl, acetylfentanyl, parafluorofentanyl, and acrylfentanyl), the CH_2 twist at C_α (benzylfentanyl), the CH_2 scissoring at C_α (acrylfentanyl), the CH_2 scissoring at C_β (parafluorofentanyl), and the CH_3 in-plane bend from the amide group (acetylfentanyl, parafluorofentanyl, and butyrylfentanyl). Furanylfentanyl had a very strong band at 1,472 cm^{-1} due to the C═C stretch in the *furane* ring, and the other six analogs had a weak to moderate band at ~1,460 cm^{-1} in NR spectra, due to the CH_2 scissoring in the *pip* ring. Fentanyl analogs had three bands in the region of 1,220–1,170 cm^{-1}. These three bands were mainly due to the CH_2 out-of-plane bend in the *pip* ring, C_α and C_β, as well as the stretch of N-alkyl chain (butyrylfentanyl, fentanyl, and parafluorofentanyl), the stretch of amide side chain (acrylfentanyl), and the bend of *pip-amide-furane group* (furanylfentanyl). At low wavenumbers, the band at ~832 cm^{-1} was related to the stretch of the *N-alkyl chain* (fentanyl, acrylfentanyl, and butyrylfentanyl), the rocking of CH_2 in *pip* (benzylfentanyl, acetylfentanyl, and acrylfentanyl), the in-plane bend of C–C–C in *pip* (acrylfentanyl), and the ring breathing of *B1* (acetylfentanyl). This strong band was shifted at ~824 cm^{-1} for parafluorofentanyl and was assigned to the out-of-plane bending of CH in *B2* and the in-plane bending of the *amide side chain*. This band was absent in furanylfentanyl, which showed instead a weak band at 886 cm^{-1}, assigned to the complex in-plane bending of C_{B2}-N2-C_ε-C_{furane} and C_{B2}-N2-C_{pip}, as well as to the out-of-plane bending of CH in *B2*. The band at ~620 cm^{-1} appeared in all fentanyl analogs and was due to the in-plane ring bending of either *B1* or *B2* or both.

Next, we compared the bands of the seven fentanyl analogs in the SERS spectra (Figure 4). The SERS spectra exhibited a smaller number of bands than the NR spectra. The previously designated fentanyl marker band at ~1,004 cm^{-1} was observed for all analogs. Butyrylfentanyl was the only analog that did not have a weak band at ~746 cm^{-1}, whereas para-fluorofentanyl had it shifted at 824 cm^{-1} and higher in intensity because of the presence of a fluorine on *B2*. Furanylfentanyl had an additional strong band at 1,468 cm^{-1} due to the presence of the furane ring. Interestingly, the double band at 1,602 and 1,586 cm^{-1} was observed to have a higher intensity on the component at 1,602 cm^{-1}, except for benzylfentanyl, in which the intensities of the two components were much closer to one another. This analog also had a wide band, which shifted from 1,442 cm^{-1} to 1,454 cm^{-1}. Acrylfentanyl had a C═C bond in the amide group, and its in-plane bending contributed to a moderate band at 1,357 cm^{-1} in the DFT spectra. It also gave a weak triple band at 1,310, 1,278, and 1,224 cm^{-1} in the SERS spectrum, with a medium intensity band at 1,276 cm^{-1}. Acetylfentanyl only had a methyl group in the amide side chain; therefore, it had a N2-C_ε-C1 stretch and a CH_3 rocking to yield a band at 652 cm^{-1} in the NR spectrum and at 660 cm^{-1} in the SERS spectrum.

3.6 | Statistical analysis

Thirteen SERS spectra from standard solutions were measured over a range of 3,278–200 cm^{-1} and 1,700–400 cm^{-1}. Data processing was performed using SPSS version 20. The PCA results are shown in Figure 5. To study the distinguishability of PC1 and PC2, descriptive

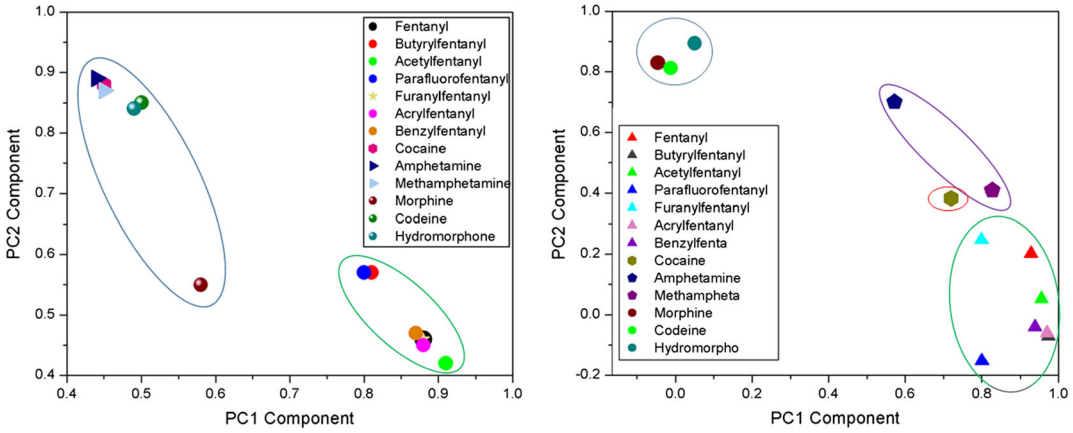

FIGURE 5 2-D principle component analysis plots showed the separation of data based on different classed of drugs of abuse. Left: analytes' spectra of 3,278–200 cm^{-1}. Right: analytes' spectra of 1,700–400 cm^{-1} [Colour figure can be viewed at wileyonlinelibrary.com]

statistics, independent-sample T tests, and nonparametric Mann–Whitney U test were used. Thirteen samples were separated into two groups of fentanyl analogs and nonfentanyl analogs.

In the range of 3,278–200 cm^{-1}, the PC1 of both groups displayed normal distributions (Shapiro–Wilk test, fentanyl. Sig = 0.089, nonfentanyl. Sig = 0.089), and they did not have unequal variance (Levene's test, F = 0.224, Sig. = 0.645). Therefore, the PC1 of fentanyl analogs (0.86 ± 0.04) was higher than nonfentanyl drugs' (0.48 ± 0.05); the difference value was 0.38 (95% CI [0.32, 0.43]). According to *t* test (t = 16.60 and $P < .0005$), PC1 can distinguish the groups of fentanyl analogs and nonfentanyl drugs. As for PC2, this group of fentanyl analogs displayed a non-normal distribution (Shapiro–Wilk test, Sig = 0.001), whereas the nonfentanyl drugs showed some outliers due to morphine (Shapiro–Wilk test, Sig = 0.057). A Mann–Whitney U test was applied to determine if there were differences in PC2 between fentanyls and nonfentanyls. The results showed that the median PC2 for fentanyls (0.46) and nonfentanyl (0.86) were statistically significantly different (U = 2, Z = −2.714, 0.005). In the range of 1,700–400 cm^{-1}, PC1 in the fentanyl analogs group displayed a non-normal distribution (Shapiro–Wilk test, Sig = 0.018), and the nonfentanyl drugs showed a normal distribution. A Mann–Whitney U test was applied to confirm that PC1 had differences between fentanyls and nonfentanyls. The median PC2 for fentanyls (0.94) and nonfentanyl (0.31) was statistically significantly different, U = 2, Z = −2.714, 0.005 using an exact sampling distribution for U. The PC2 of both groups displayed normal distributions (Shapiro–Wilk test, fentanyl. Sig = 0.357, nonfentanyl. Sig = 0.138), and they did show unequal variance (Levene's test, F = 1.836, Sig. = 0.203). Therefore, PC2 of fentanyl analogs (0.03 ± 0.15) was lower than nonfentanyl drugs' (0.67 ± 0.22), and the difference value was −0.64 (95% CI [−0.87, −0.42). According to *t* test, $t = -6.235$ and $P < 0.0005$, PC2 can distinguish between the groups of fentanyl analogs and nonfentanyl drugs. Therefore, the PC1 and PC2 loadings revealed that fentanyl analogs and nonfentanyl drugs can be distinguished by SERS spectra.

4 | CONCLUSIONS

We have examined fentanyl and its six analogs using geometrical optimization and calculation of vibrational frequencies and Raman activities within DFT at the wB97XD/cc-pVTZ level. The assignment of the Raman and SERS vibrational bands of fentanyl analogs was accomplished based on these theoretical calculations. Our results demonstrate that NR spectroscopy can be useful in the identification of crystalline fentanyl analogs, whereas SERS can detect a lower concentration of fentanyl analogs in solution. The PCA results demonstrate the capability of Raman spectroscopy and SERS to distinguish and characterize a variety of fentanyl analogs.

ACKNOWLEDGEMENTS

The authors would like to acknowledge NSF IUCRC award 1739805 to FIU—Center for Advanced Research in Forensic Science.

ORCID

Chiara Deriu https://orcid.org/0000-0003-3077-5029
Bruce McCord https://orcid.org/0000-0002-8366-1925

REFERENCES

[1] T. H. Stanley, *J. Pain Symptom Manage.* **1992**, *7*, 3.
[2] L. P. Tamburro, J. H. Al-Hadidi, L. J. Dragovic, *J. Forensic Sci. Med.* **2016**, *2*, 2.
[3] A. Poklis, *J. Toxicol. Clin. Toxicol.* **1995**, *33*, 5.
[4] J. K. O'Donnell, J. Halpin, C. L. Mattson, B. A. Goldberger, R. M. Gladden, *MMWR Morb. Mortal. Wkly Rep.* **2017**, *66*, 43.
[5] D. A. Algren, C. P. Monteilh, M. Punja, J. G. Schier, M. Belson, B. R. Hepler, M. Straetemans, *J. Med. Toxicol.* **2006**, *9*, 1.
[6] https://www.drugabuse.gov/news-events/news-releases/2018/05/nearly-half-opioid-related-overdose-deaths-involve-fentanyl (accessed on 6/12/2018)
[7] C. M. Jones, E. B. Einstein, W. M. Compton, *JAMA* **2018**, *319*, 17.
[8] https://www.federalregister.gov/documents/2018/02/06/2018-02319/schedules-of-controlled-substances-temporary-placement-of-fentanyl-related-substances-in-schedule-i (accessed on 6/12/2018)
[9] L. J. Marinetti, B. J. Ehlers, *J. Anal. Toxicol.* **2014**, *38*, 8.
[10] UNODC, Recommended methods for the identification and analysis of fentanyl and its analogues in biological specimens, Vienna, **2017**
[11] M. L. Snyder, P. Jarolim, S. E. Melanson, *Clin. Chim. Acta* **2011**, *412*, 11.
[12] E. Sisco, J. Verkouteren, J. Staymates, J. Lawrence, *Forensic Chem.* **2017**, *4*, 108.
[13] N. F. Van Nimmen, K. L. Poels, H. A. Veulemans, *J. Chromatogr. B* **2004**, *804*, 2.
[14] S. Strano-Rossi, A. M. Bermejo, X. De La Torre, F. Botre, *Anal. Bioanal. Chem.* **2011**, *399*, 4.
[15] S. Farquharson, C. Shende, A. Sengupta, H. Huang, F. Inscore, *Pharmaceutics* **2011**, *3*, 3.
[16] J. Leonard, A. Haddad, O. Green, R. L. Birke, T. Kubic, A. Kocak, J. R. Lombardi, *J. Raman Spectrosc.* **2017**, *48*, 10.

[17] A. Haddad, M. A. Comanescu, O. Green, T. A. Kubic, J. R. Lombardi, *Anal. Chem.* **2018**, *90*, 12678.

[18] A. L. Mohr, M. Friscia, D. Papsun, S. L. Kacinko, D. Buzby, B. K. Logan, *J. Anal. Toxicol.* **2016**, *40*, 9.

[19] N. H. Huynh, N. Tyrefors, L. Ekman, M. Johansson, *J. Pharm. Biomed. Anal.* **2005**, *37*, 5.

[20] R. Gupta, R. Verma, J. Bogra, M. Kohli, R. Raman, J. K. Kushwaha, *J. Anaesthesiol Clin. Pharmacol.* **2011**, *27*, 3.

[21] S. He, M. W. C. Kang, F. J. Khan, E. K. M. Tan, M. A. Reyes, J. C. Y. Kah, *J. Opt.* **2015**, *17*, 11.

[22] M. J. Frisch, G. W. Trucks, H. B. Schlegel, G.E. Scuseria, M.A. Robb, J.R. Cheeseman, G. Scalmani, B. Mennucci, G.A. Petersson, H. Nakatsuji, Gaussian 09, revision B.01, Gaussian, Inc.: Wallingford, CT. **2010**.

[23] A. D. Becke, *J. Chem. Phys.* **1993**, *98*, 7.

[24] C. Lee, W. Yang, R. G. Parr, *Phys. Rev.* **1988**, *37*, 2.

[25] J.-D. Chai, M. Head-Gordon, *J. Chem. Phys.* **2008**, *128*, 8.

[26] T. H. Dunning, *J. Chem. Phys.* **1989**, *90*, 2.

[27] L. Tian, F. Chen, *J. Comput. Chem.* **2012**, *33*, 5.

[28] G. Schaftenaar, J. H. Noordik, *J. Comput. Aided Mol. Des.* **2000**, *14*, 2.

[29] A. P. Scott, L. Radom, *J. Phys. Chem.* **1996**, *100*, 41.

[30] M. A. Palafox, *J. Phys. Chem.* **1999**, *103*, 51.

[31] M. V. Canamares, J. V. Garcia-Ramos, J. D. Gomez-Varga, C. Domingo, S. Sanchez-Cortes, *Langmuir* **2005**, *21*, 18.

SUPPORTING INFORMATION

Additional supporting information may be found online in the Supporting Information section at the end of the article.

How to cite this article: Wang L, Deriu C, Wu W, Mebel AM, McCord B. Surface-enhanced Raman spectroscopy, Raman, and density functional theoretical analyses of fentanyl and six analogs. *J Raman Spectrosc*. 2019;1–11. https://doi.org/10.1002/jrs.5656